

## Effects of bifurcations on the energy level statistics for oval billiards

H. Makino,<sup>1</sup> T. Harayama,<sup>2</sup> and Y. Aizawa<sup>1</sup>

<sup>1</sup>*Department of Applied Physics, Waseda University, 3-4-1 Okubo, Shinjuku-ku, Tokyo 169-0072, Japan*

<sup>2</sup>*ATR Adaptive Communications Research Laboratories, 2-2 Hikaridai, Seika-cho, Soraku-gun, Kyoto 619-02, Japan*

(Received 17 September 1998; revised manuscript received 3 December 1998)

We studied the energy level statistics for one parameter family of oval billiards whose classical phase space consists of some regular and some irregular components. As the parameter is varied, a transition from an integrable system to a strongly chaotic one occurs with successive bifurcations. We applied the Berry-Robnik formula to the level-spacing distributions for a variety of shapes of quantum oval billiards and found some striking effects of bifurcations in the classical mechanical systems on the level-spacing distributions. The validity of the Berry-Robnik formula is also checked for those shapes of the oval billiard for which there exist two separated chaotic components in the phase space. [S1063-651X(99)03304-8]

PACS number(s): 05.45.Mt, 03.65.Sq

### I. INTRODUCTION

An important feature of the quantum system appears in the statistical properties of energy levels. It is widely known that the level-spacing distribution of an integrable system is characterized by the Poisson distribution [1,2] while a strongly chaotic system is characterized by the Wigner distribution [3]. Continuous changes shifting the Poisson distribution toward the Wigner distribution have been observed in mixed systems, where the volume ratio of regular and irregular components in classical phase space is controlled by a system parameter [4–6]. Berry and Robnik have provided a formula for the level-spacing distributions in mixed systems [7]. Their formula depends sensitively on the volume ratio of irregular components, which is strongly affected by the bifurcations. This means that bifurcations in classical-mechanical systems affect the energy level statistics of the corresponding quantum systems. The validity of the Berry-Robnik formula has been checked by numerical calculations for several systems [8–18].

In this paper, using the Berry-Robnik formula, we show the effects of bifurcations in the classical oval billiard systems on the level-spacing distributions of the quantum oval billiards. The oval billiard was introduced by Benettin and Strelcyn [20], and studied in detail by Henon and Wisdom [21]. The shape of the billiard depends on the value of a certain parameter. The phase space of the classical-mechanical system consists of regular and irregular components, which correspond to tori and chaos, respectively. As the parameter is varied, transitions occur from the integrable to the strongly chaotic system. The transition is accompanied by bifurcations, e.g., the creation and the disappearance of periodic orbits which affect the volume ratios of regular and irregular components.

The present paper is organized as follows. The oval billiard is introduced in Sec. II A. In Sec. II B, the Poincaré surface of section for the oval billiard is defined, and the bifurcation is also explained. In Sec. II C, we show our method used in the direct measurement of the phase volume  $\rho_i$  for various components ( $i=1,2,3,\dots,K$ ) in classical phase space. The level-spacing distributions are given in Sec. III A, where the Berry-Robnik formula is successfully ap-

plied and the effects of bifurcations on the energy level statistics are precisely analyzed in Secs. III B and III C.

### II. CLASSICAL MECHANICS

#### A. Oval billiards

Figure 1 shows the schematic definition of the oval billiard. The wall  $\partial D$  for the oval billiard is constructed as follows. In a rectangular system of coordinates  $(x,y)$ , we consider four points  $P_1, P_2, P_3,$  and  $P_4$  with coordinates  $(1,1), (-1,1), (-1,-1),$  and  $(1,-1)$  forming a square with side length 2. Let the point  $O_1$  with coordinate  $(1-\delta,0)$  be the center of an arc  $\widehat{P_4P_1}$ , where  $\delta$  is defined in the interval  $0 \leq \delta \leq 1$ .  $O_2$  is an intersection of the extension line of  $P_1O_1$  and the  $y$  axis, and is the center of an arc  $\widehat{P_1P_2}$ . The wall  $\partial D$  of the billiard consists of the above two arcs and another two arcs,  $\widehat{P_2P_3}$  and  $\widehat{P_3P_4}$ , constructed like  $\widehat{P_4P_1}$  and  $\widehat{P_1P_2}$ . The initial condition of the motion of a particle is determined by its position and direction. In the case  $\delta=1$ , the shape of the billiard wall is circular, and hence the motion of the particle is regular, i.e., the billiard system is completely integrable. On the other hand, in the case  $\delta=0$ , the shape of the billiard wall corresponds to a stadium and the motion of the particle is irregular, i.e., the billiard system is a  $K$  system, or strongly

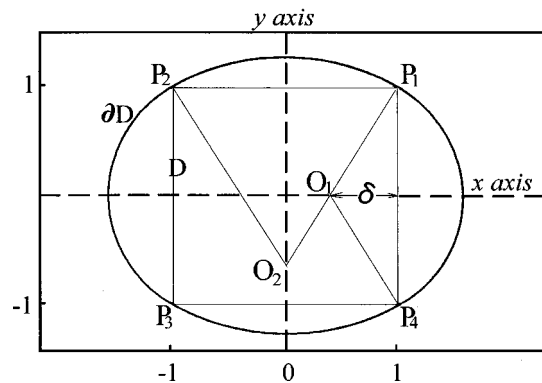


FIG. 1. Schematic picture of the oval billiard whose boundary wall consists of four circular arcs.

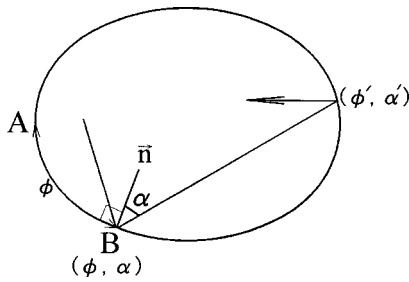


FIG. 2. Definition of the Birkhoff coordinates  $(\phi, \sin(\alpha))$ .

chaotic system [22]. Thus one can see a continuous change from the integrable case to the nonintegrable case as the parameter  $\delta$  is varied from 1 to 0. In the case of an intermediate parameter regime  $0 < \delta < 1$ , the motion can be regular or irregular, depending on the initial condition.

**B. Poincaré surface of section**

We consider the successive collisions of a particle with the wall  $\partial D$  and define the Birkhoff coordinates  $(\phi, \sin(\alpha))$  as shown in Fig. 2, where  $\phi$  is the curvilinear distance measured along the wall from the origin  $A$  to the collisional point  $B$ , and  $\alpha$  is the angle between the inner normal and the orbit reflected from the wall  $\partial D$ . The Birkhoff coordinates defined

in Fig. 2 are the most natural representation of a Poincaré surface of section for billiard systems and describe the global behavior of motions [23].

Figure 3 shows the trajectories in the Birkhoff coordinates for various values of  $\delta$ . In the case of the stadium ( $\delta=0$ ) and the circle ( $\delta=1$ ), the whole surface of the section is completely filled with irregular and regular orbits, respectively. In all cases that  $0 < \delta < 1$ , regular and irregular components coexist in the Poincaré surface of section.

As  $\delta$  increases from 0, one can observe the gradual enhancement of regular components around two elliptic fixed points,  $(\phi, \sin(\alpha)) = (0.25, 0)$  and  $(0.75, 0)$ , as shown in Figs. 3(a)–3(e). But the sizes of these two largest islands suddenly change at the critical point  $\delta = \delta_{c1}$ ,

$$\delta_{c1} = \sqrt{2} - 1 = 0.414\ 213\ 56 \dots, \tag{2.1}$$

where a hyperbolic periodic orbit bounces just on the joints of the billiard wall  $P_i$  ( $\phi = \phi_i$ ), as shown in Fig. 5(a). One can see the sudden enhancement of the two largest islands around  $\delta = \delta_{c1}$ , as shown in Figs. 4(a) and 4(b).

As  $\delta$  increases further, the hyperbolic periodic orbits mentioned above invade into the neighboring regions on the Poincaré surface,  $\phi_1 < \phi < \phi_2$  and  $\phi_3 < \phi < \phi_4$ , as shown in Figs. 4(a)–4(e). This invasion process induces the increase

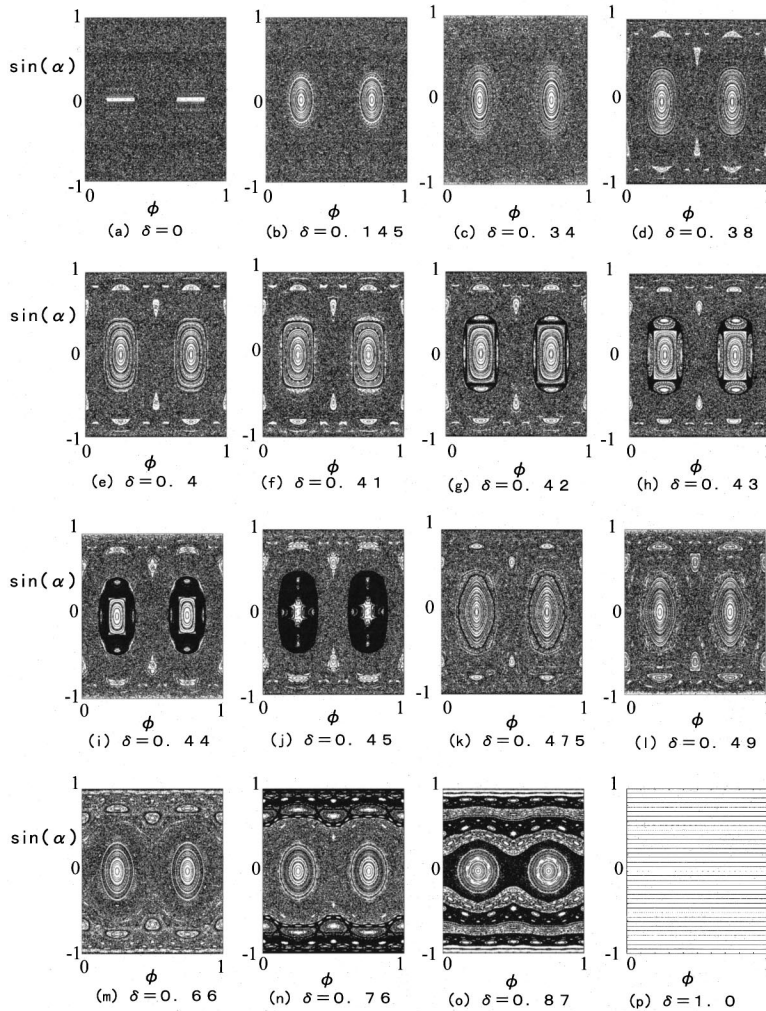


FIG. 3. Poincaré surface of section for various values of  $\delta$ .

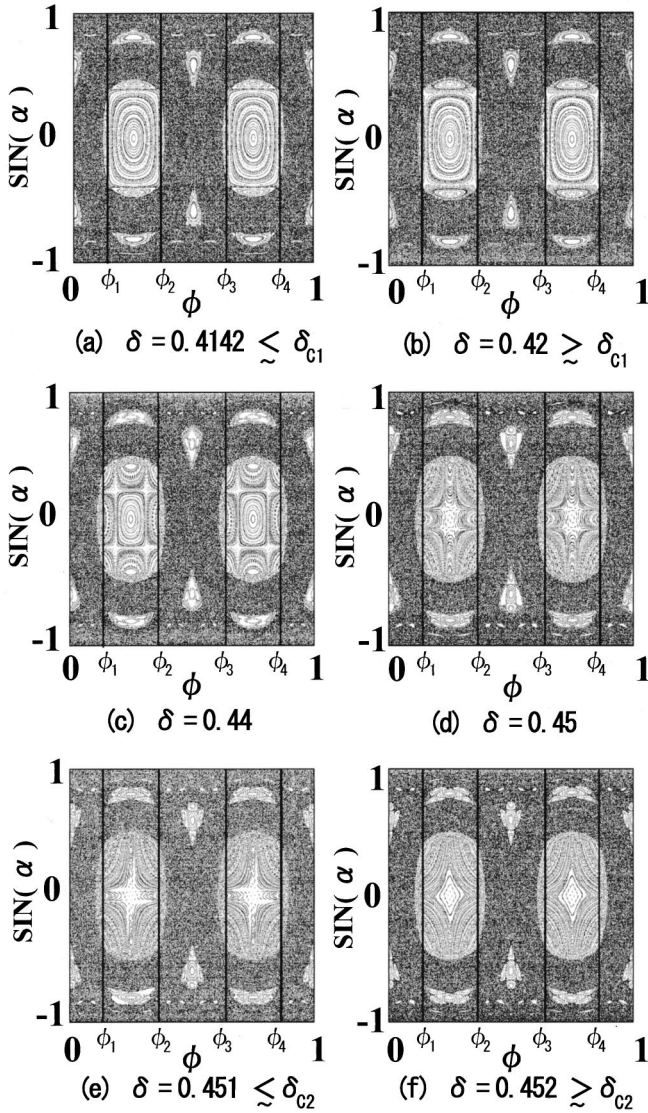


FIG. 4. Poincaré surface of section near the bifurcation point  $\delta = \delta_{c2} = 0.45141623\dots$ . The solid lines represent the joints of the billiard wall  $P_i (i=1, \dots, 4)$ .

of the second irregular components inside the two largest islands, as shown in Figs. 3(g)–3(j). When  $\delta$  equals another critical point  $\delta_{c2}$ ,

$$\delta_{c2} = \frac{4 - \sqrt{7}}{3} = 0.451416229\dots, \quad (2.2)$$

an elliptic periodic orbit, with a period of 4, bounces just on the joints of the billiard wall as shown in Fig. 5(b). Here one can see a bifurcation where the elliptic periodic points suddenly disappear, and, simultaneously, hyperbolic periodic points collide with other elliptic points at  $(\phi, \sin(\alpha)) = (0.25, 0)$  and  $(0.75, 0)$ , as shown in Figs. 4(e) and 4(f). Thus another elliptic periodic point with a period of 2 is created. Around  $\delta = 0.47$ , the second irregular components mentioned above disappear through the destruction of their outermost boundary surfaces [24], and as a result, the volume of the regular regions increases again. The coexistence of the different irregular regions causes remarkable effects

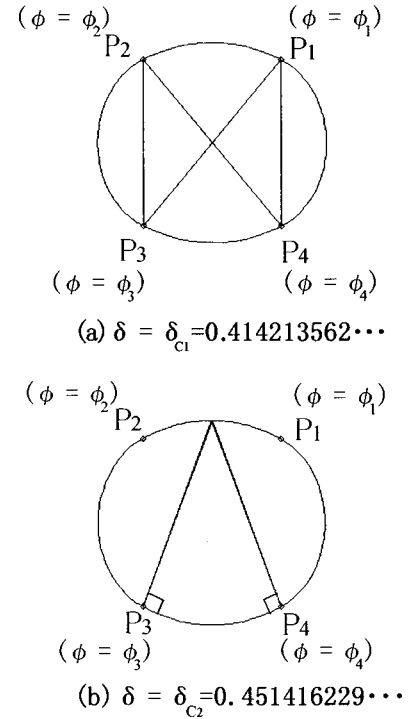


FIG. 5. (a) An unstable periodic orbit with a period of 4 bouncing on the joints of the billiard wall  $P_i (\phi = \phi_i)$  at  $\delta = \delta_{c1} = 0.41421356\dots$ . (b) A stable periodic orbit with a period of 4 bouncing on the same joints  $P_i (\phi = \phi_i)$  at  $\delta = \delta_{c2} = 0.45141623\dots$ .

on the statistical properties of the corresponding quantum system. These points will be discussed in Sec. III C.

When  $\delta > 0.76$ , the irregular regions are divided into two or more components by many transversal invariant tori as shown in Figs. 3(n) and 3(o) [20,21]. As  $\delta$  approaches 1, the number of chaotic components becomes infinite, because almost all transversal invariant tori remain stable in off-resonant regions.

### C. Estimation of chaotic regions

Here we provide a numerical method to estimate the area of the irregular component on the Poincaré surface of section. In order to judge the regularity of the trajectory, the rotation number  $R_N$  is calculated numerically for each initial point,

$$R_N = \frac{\sum_{i=1}^N (\theta_{i+1} - \theta_i)}{2\pi N}, \quad (2.3)$$

where  $\theta_i$  is the angle of the  $i$ th iterated motion oriented anticlockwise from the  $x$  axis of the rectangular coordinate as shown in Fig. 6(a), and  $N$  is the number of collisions. Figure 6(b) shows that the value of  $R_N$  converges more rapidly in the case of regular motions than in the case of irregular motions. Let us define the regularity or the irregularity of the trajectory by the convergence speed of the rotation number  $R_N$ . The convergence of  $R_N$  is characterized by the partial mean  $Z_N$  as follows:

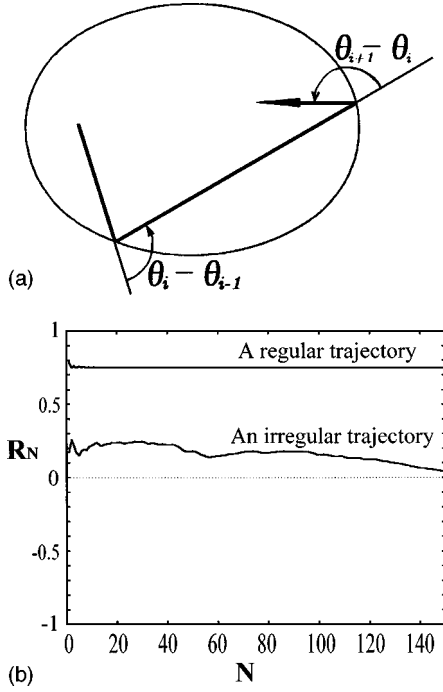


FIG. 6. (a) Definition of the rotation angle  $\theta_i$ . (b) Rotation number  $R_N$  versus  $N$  for a regular and an irregular trajectory.  $N$  is the number of iterations.

$$Z_N = \frac{|R_N - \overline{R_N}|}{|\overline{R_N}|}, \quad (2.4)$$

where

$$\overline{R_N} = \frac{\sum_{i=1}^N R_i}{N}. \quad (2.5)$$

Note that the value of  $Z_N$  converges to 0 when  $N$  goes to infinity. It is clear that the value of  $Z_N$  converges to 0 more rapidly in the case of regular trajectory than in the case of irregular trajectory. Due to the symmetry of the surface of section, it is sufficient to deal with the region defined by  $0 \leq \alpha \leq \pi/2$ ,  $0 \leq \phi \leq \frac{1}{4}$ . This region on the surface of section is divided into  $400 \times 300$  grid cells. An initial point is put at the center of each cell. Figure 7 shows the distribution  $\tilde{P}(Z_{500})$ , of the partial means  $Z_{500}$  at  $\delta=0.38$ . There are two peaks in the distribution function  $\tilde{P}(Z_{500})$ , because it is a superposition of two independent distributions; one is very sharp and located near the origin of  $Z_{500}$ , and the other is broad. The former peak corresponds to the contributions of regular trajectories and the latter to those of irregular trajectories. Note that the distribution  $\tilde{P}(Z_N)$  always has two peaks. Therefore the threshold value  $Z_N^c$ , which gives the minimum of  $\tilde{P}(Z_N)$ , enables us to classify the initial points into two parts as follows:

$$Z_N \leq Z_N^c \Rightarrow \text{regular trajectory},$$

$$Z_N > Z_N^c \Rightarrow \text{irregular trajectory}.$$

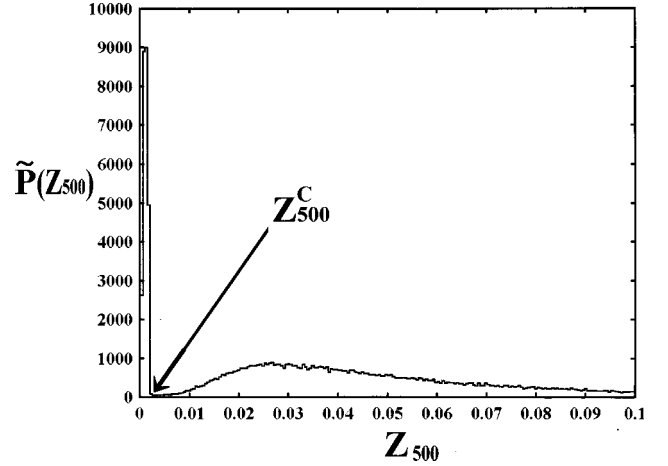


FIG. 7. Distribution function  $\tilde{P}(Z_{500})$  at  $\delta=0.38$ . The vertical axis represents the number of orbits initialized at the center of each cell in the Poincaré surface of section. The criterion  $Z_{500}^c$  is chosen at the minimum point between the peaks.

The ratio of the regular components  $\rho_1$  and that of the irregular ones  $\rho_2$  are determined by

$$\rho_1 = \frac{\int_0^{Z_N^c} \tilde{P}(Z_N) dZ_N}{\int_0^\infty \tilde{P}(Z_N) dZ_N}, \quad \rho_2 = \frac{\int_{Z_N^c}^\infty \tilde{P}(Z_N) dZ_N}{\int_0^\infty \tilde{P}(Z_N) dZ_N}. \quad (2.6)$$

The value of  $\rho_2$  in the case of  $N=10^5$  is shown in Figs. 11 and 13.

Our numerical method shown in this section is quite different from traditional ones which require calculation of the local Lyapounov exponents. Here, we will just give a numerical evidence for the justification of our method. Figure 8(a) shows a plot of “irregular cells” on the Poincaré surface of section which are determined by our method for the case of  $\delta=0.38$  and  $N=500$ . One can easily see that our method works very well, and it reproduces almost completely the irregular region in Fig. 8(b).

### III. QUANTUM MECHANICS

#### A. The energy level statistics and the Berry-Robnik formula

In this section, the statistical properties of the quantum system corresponding to the oval billiard are investigated. The energy levels are obtained by solving numerically the Schrödinger-Helmholtz equation,

$$\nabla^2 \psi(\mathbf{r}) + \frac{2mE}{\hbar^2} \psi(\mathbf{r}) = 0, \quad (3.1)$$

under the Dirichlet boundary condition  $\psi(\mathbf{r} \in \partial D) = 0$ . Here  $\hbar$  is the Plank constant,  $E$  the eigenenergy,  $m$  the mass of the particle, and  $\psi(\mathbf{r})$  the corresponding eigenfunction. Equation (3.1) is solved effectively by the boundary element method [25,26].

Figure 9 shows  $\delta$  dependence of the energy levels. As  $\delta$  approaches 0 where the classical-mechanical system is strongly chaotic, one can see a number of avoided crossings

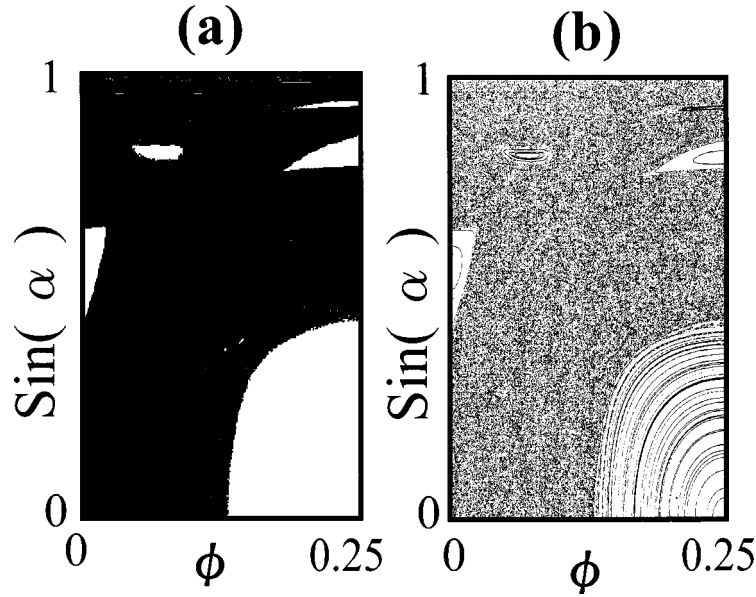


FIG. 8. (a) Poincaré plots for the case  $\delta=0.38$  and  $N=500$  reproduced by our method mentioned in Sec. III C. Dark region stands for “irregular cells” and white for “regular ones.” (b) Poincaré surface of section obtained by numerical plots for  $\delta=0.38$ .

(or level repulsions). At  $\delta=1$  where the classical-mechanical system is integrable, several accidental degeneracies occur. The effect of level repulsions can be characterized by the level-spacing distribution  $P(S)$  [1], where  $S$  denotes the nearest level spacing. The energy levels are unfolded to fix the mean spacing unity. Figure 10 shows the level-spacing distribution  $P(S)$  for various values of  $\delta$ . We deal with 2650 energy levels which belong to the even-even parity of the eigenstates, but the lower 100 levels are omitted because of the semiclassical consideration.

When the shape of the billiard wall is a circle ( $\delta=1$ ),  $P(S)$  is well approximated by the Poisson distribution, i.e.,  $P_{\text{Poisson}}(S) = \exp(-S)$ . On the other hand, in the strongly chaotic case of the stadium ( $\delta=0$ ),  $P(S)$  corresponds to the Wigner distribution  $P_{\text{Wigner}}(S) = \frac{1}{2} \pi S \exp(-\pi S^2/4)$ . In the intermediate case ( $0 < \delta < 1$ ), the distribution  $P(S)$  exhibits systematic deviations from those two distributions, as shown in Figs. 10(a)–10(h). In what follows, the level-spacing distributions  $P(S)$  in the mixed systems will be analyzed in accordance with the basic idea proposed by Berry and Robnik [7].

Let us review briefly the distribution of the Berry-Robnik formula. Consider a system whose classical phase space (or

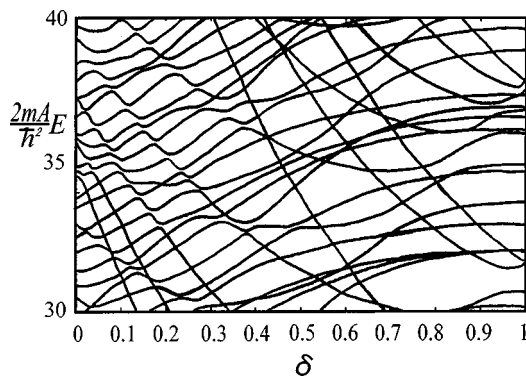


FIG. 9. Some levels of the eigenenergy.  $A$  is area of inner domain in the oval billiards.

Poincaré surface of section) is decomposed into regular and irregular components, and denote the total volume ratio of the regular components by  $\rho_1$  and the volume ratios of disconnected chaotic components by  $\rho_i$  ( $i=2,3,4,\dots,K$ ). Percival conjectured that in the semiclassical limit, the energy levels consist of regular and irregular parts having strongly contrasting properties [27]. Berry and Robnik extended this conjecture, and surmised that the sequence of the energy levels of a mixed system is given by the superposition of statistically independent sequences corresponding to the classical phase-space components: the distributions of the sequences corresponding to regular and irregular regions are,

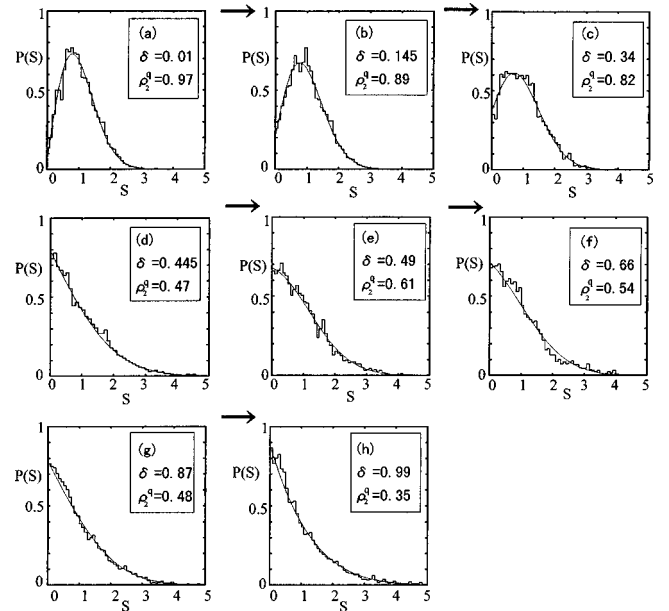


FIG. 10. Numerical results of the level-spacing distribution  $P(S)$  for various values of  $\delta$ . In each case, 2550 level spacings which belong to even-even parity are used and the best-fitting curve of the Berry-Robnik formula [Eq. (3.3)] is shown by the solid line with parameter  $\rho_1^q$ .

respectively, the Poisson and Wigner distributions [7]. The statistical independence of each subsequence in the semiclassical limit is justified by the *principle of uniform semiclassical condensation of eigenstates* onto each component of the classical phase space and by the lack of their mutual overlap [14,28,18,19]. Thus one can obtain the Berry-Robnik formula which describes the level-spacing distribution for mixed systems,

$$P_K^{\text{BR}}(\rho_1, \rho_2, \dots, \rho_K; S) = \frac{d^2}{dS^2} \left[ \exp(-\rho_1 S) \prod_{i=2}^K \text{erfc} \left( \frac{\sqrt{\pi}}{2} \rho_i S \right) \right], \quad (3.2)$$

where

$$\text{erfc}(x) = \frac{2}{\sqrt{\pi}} \int_x^\infty \exp(-t^2) dt.$$

Many numerical tests of the Berry-Robnik formula have been done for mixed systems having only one irregular component (i.e.,  $K=2$ ) [14]. In particular, Prosen and Robnik [10] and Prosen [18] have numerically shown the validity of the Berry-Robnik formula in an extremely deep semiclassical limit using a large number of energy levels. However, only a few attempts have been made thus far with the mixed systems having many chaotic components ( $K \geq 3$ ) [11].

### B. The effect of bifurcations on level-spacing distributions

When there exists only a single chaotic component in the classical phase space, Eq. (3.2) is rewritten into

$$P_{K=2}^{\text{BR}}(\rho_1, \rho_2; S) = \left[ \rho_1^2 \text{erfc} \left( \frac{\sqrt{\pi}}{2} \rho_2 S \right) + \left( 2\rho_1 \rho_2 + \frac{\pi}{2} \rho_2^3 S \right) \exp \left( -\frac{\pi}{4} \rho_2^2 S^2 \right) \right] \times \exp(-\rho_1 S), \quad (3.3)$$

where  $\rho_1 + \rho_2 = 1$ . Here we use  $P_{K=2}^{\text{BR}}(\rho_1, \rho_2; S)$  as the measure for the effect of bifurcations on the level-spacing distributions.  $P_{K=2}^{\text{BR}}(\rho_1, \rho_2; S)$  approximates very well the level-spacing distribution of the mixed system even if the chaotic components are multiple. Figure 10 gives the best-fit curve of the level-spacing distribution  $P(S)$  by the Berry-Robnik formula of Eq. (3.3), where the parameter  $\rho_2^q$  is determined by the least squares method for the cumulative level-spacing distribution  $W(S) = \int_0^S P(S') dS'$ . Figure 11 shows  $\rho_2^q$  versus  $\delta$ . 2550 level spacings are used for each value of  $\delta$ , and 3500 level spacings are used near the bifurcation point  $0.41 \leq \delta \leq 0.48$ . Notably, there exists a sudden decrease of  $\rho_2^q$  around the bifurcation point  $\delta_{c2}$ , where two chaotic components coexist in the phase space.

It is also important that the values of  $\rho_2^q$  around  $\delta_{c2}$  are not equal to  $\rho_2$  values, which are the ratios of chaotic components and are determined only by the classical-mechanical information as we explained in Sec. II. Figure 11 compares values  $\rho_2^q$  and  $\rho_2$  for various values of  $\delta$ . One can see that

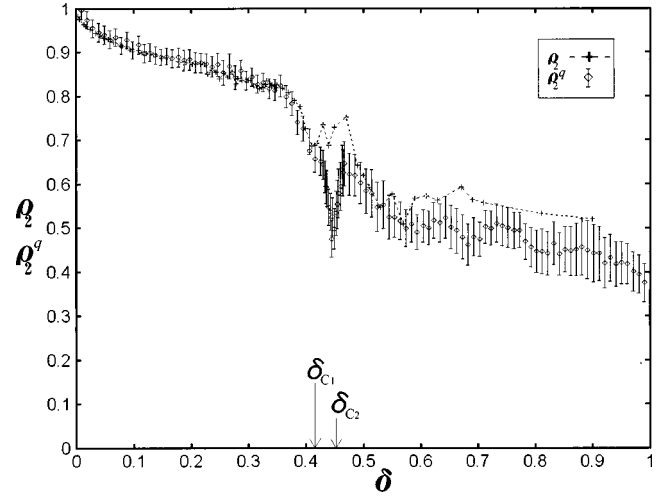


FIG. 11. Comparison between  $\rho_2$  and  $\rho_2^q$  for the whole region of the parameter values of  $\delta$ . The error bars indicate the statistical fluctuations due to the finite size effect of ensembles.

very nice agreement is obtained near the completely irregular limit  $\delta=0$ . However, a remarkable difference appears at  $\delta \approx \delta_{c2}$  ( $0.41 \leq \delta \leq 0.47$ ). Here we have to remember that the classical-mechanical system exhibits very complicated bifurcations in the same parameter regime as shown in Figs. 3(f)–3(j) and 4(a)–4(f). The reason for this disagreement should be explained by using the general form of Eq. (3.2) instead of that of Eq. (3.3). Indeed, it will be shown in the next section that the dip structure of  $\rho_2^q$  shown in Fig. 11 comes from the effects of the bifurcations in the classical-mechanical system.

Furthermore, the disagreement of  $\rho_2$  and  $\rho_2^q$  is also observed near the integrable limit  $\delta=1$  as shown in Fig. 11. The same disagreement has also been pointed out in several previous papers [8,15]. From the viewpoint of classical mechanics in the neighborhood of the completely integrable limit  $\delta=1$ , there appear a number of Kol'mogorov-Arnol'd-Moser (KAM) tori which divide the irregular regions into many pieces, as shown in Figs. 3(n) and 3(o) [20,21]. Here we have to use the general form of Eq. (3.2) with  $K \rightarrow \infty$ . Remarkable changes of  $\rho_2^q$  are expected to appear near each of the division points  $\delta \approx 0.76, 0.85, \dots$ . However, the effects of these divisions on  $\rho_2^q$  are not observed clearly in our numerical calculations. This is because one can never obtain enough condensation of the eigenstates in the neighborhood of  $\sin \alpha \approx \pm 1$  in the low energy region [29]. In the present paper, our main concerns will be the bifurcation at  $\delta \approx \delta_{c2}$ , where at least two disjoint irregular components contribute to the Berry-Robnik formula ( $K=3$ ).

### C. The Berry-Robnik formula for two chaotic components

As shown in Fig. 11, a remarkable difference appears between  $\rho_2$  and  $\rho_2^q$  near  $\delta = \delta_{c2}$  where bifurcations are observed in the classical-mechanical systems. The bifurcations induce the growth of the second irregular component inside the two largest islands as shown in Figs. 3(f)–3(j). Let us consider the Berry-Robnik formula in the form of  $P_{K=3}^{\text{BR}}(\rho_1^*, \rho_2^*, \rho_3^*; S)$  rather than  $P_{K=2}^{\text{BR}}(\rho_1, \rho_2; S)$ , where  $\rho_i^*$  ( $i=1,2,3$ ) is the ratio of the  $i$  component defined on the

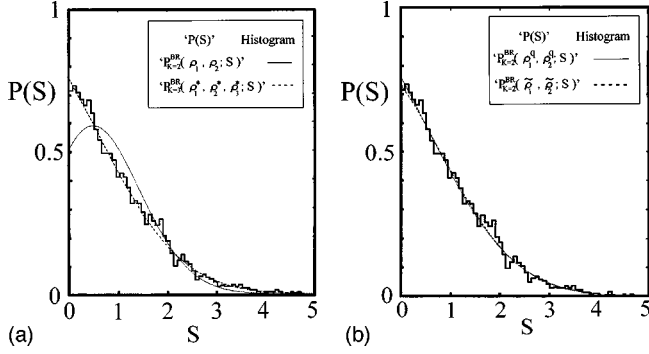


FIG. 12. (a)  $P(S)$  is numerical result of the level-spacing distribution at  $\delta=0.445$  obtained by 3500 energy levels,  $P_{K=2}^{\text{BR}}(\rho_1, \rho_2; S)$  and  $P_{K=3}^{\text{BR}}(\rho_1^*, \rho_2^*, \rho_3^*; S)$  are the Berry-Robnik formulas obtained from the classical-mechanical system. ( $\rho_1=0.3$ ,  $\rho_2=\rho_2^*+\rho_3^*=0.70$ :  $\rho_1^*=0.30$ ,  $\rho_2^*=0.468$ ,  $\rho_3^*=0.232$ .) (b) Comparison between  $P_{K=2}^{\text{BR}}(\tilde{\rho}_1, \tilde{\rho}_2; S)$  and  $P_{K=2}^{\text{BR}}(\rho_1^q, \rho_2^q; S)$  at ( $\tilde{\rho}_1=0.481$ ,  $\tilde{\rho}_2=0.519$ :  $\rho_1^q=0.505$ ,  $\rho_2^q=0.495$ ) which are obtained from the least squares method Eq. (3.4).  $P(S)$  is also plotted.

Poincaré surface of section, and satisfies  $\rho_1^*=\rho_1$  and  $\rho_2^*+\rho_3^*=\rho_2$ . The argument  $\rho_3^*$  is the volume ratio of the second irregular component, and its behavior around the bifurcation point is shown in Fig. 13(b). It should be noted that the sudden decrease of  $\rho_2^q$  at  $\delta\approx\delta_{c2}$  agrees well with the increase of the second irregular component induced by the bifurcation.

Figure 12(a) shows the numerical data of the level-spacing distribution  $P(S)$  at  $\delta=0.445$ . The Berry-Robnik formulas  $P_{K=2}^{\text{BR}}(\rho_1, \rho_2; S)$  and  $P_{K=3}^{\text{BR}}(\rho_1^*, \rho_2^*, \rho_3^*; S)$  are also plotted in the same figure. It is quite surprising that the numerical result of the level-spacing distribution  $P(S)$  is almost completely adjusted by the Berry-Robnik formula with  $K=3$ . This implies that the Berry-Robnik formula approximates the numerical data of the level-spacing distribution very closely, provided that many irregular components are taken precisely into account. Indeed, the detailed information of the classical-mechanical systems enables us to explain the sudden change of the parameters of  $\rho_i^q$ 's at  $\delta\approx\delta_{c2}$ .

Now we discuss the behavior of  $\rho_i^q$ . Let us consider the following least squares method, which gives the approximated values  $\rho_i^q$  by using only classical-mechanical information. The modified parameter  $\tilde{\rho}_i$  is obtained from the renormalization process as follows:

$$\tilde{\rho}_i = x_i \left( \int_0^\infty |P_{K=2}^{\text{BR}}(x_1, x_2; S) - P_{K=3}^{\text{BR}}(\rho_1^*, \rho_2^*, \rho_3^*; S)|^2 dS = \text{minimum} \right), \quad (3.4)$$

where  $x_1+x_2=1$ , and  $\tilde{\rho}_i$ 's are their extremum solutions ( $\tilde{\rho}_1+\tilde{\rho}_2=1$ ) subordinated to classical-mechanical information ( $\rho_1^*, \rho_2^*, \rho_3^*$ ). Figure 12(b) shows that the parameters  $\rho_i^q$  with  $K=2$  are well reproduced by  $\tilde{\rho}_i$ 's, where the volume ratios of three components ( $\rho_1^*, \rho_2^*, \rho_3^*$ ) are renormalized into two parameters ( $\tilde{\rho}_1, \tilde{\rho}_2$ ). Figures 13(a) and 13(b) exhibit that the renormalized Berry-Robnik formula with  $K=2$ , i.e.,  $P_{K=2}^{\text{BR}}(\tilde{\rho}_1, \tilde{\rho}_2; S)$ , well approximates the quantum-mechanical

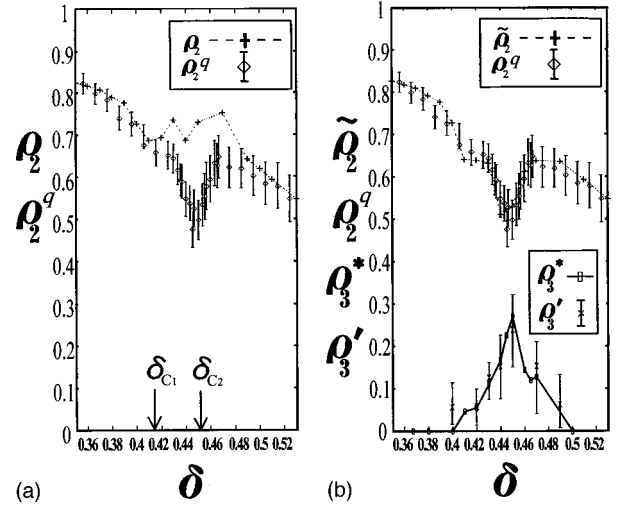


FIG. 13. (a) Comparison between  $\rho_2$  and  $\rho_2^q$  near the bifurcation point  $\delta=\delta_{c2}$ . 3500 level spacings are used for each value of  $\rho_2^q$ . (b) Comparison between  $\tilde{\rho}_2$  and  $\rho_2^q$ , and between  $\rho_3^*$  and  $\rho_3^q$  in the same parameter range.

data of level-spacing  $P(S)$  in a wide parameter region. In other words, the numerical result exhibits the following:

$$\rho_i^q(\delta) \approx \tilde{\rho}_i(\delta) \quad (i=1,2). \quad (3.5)$$

It is noteworthy that the renormalized parameters  $\tilde{\rho}_i$  completely describe the quantum-mechanical aspects induced by the bifurcations in classical-mechanical systems.

In the next section, the idea mentioned above will be extended, and it will be shown that the classical-mechanical parameters ( $\rho_1^*, \rho_2^*, \rho_3^*$ ) can be derived from the quantum-mechanical information of the level-spacing distribution  $P(S)$ .

#### D. The quantum-classical correspondence of the Berry-Robnik parameters

Let us consider the parameter region near  $\delta=\delta_{c2}$ , where three characteristic parameters ( $\rho_1, \rho_2, \rho_3$ ) play an essential role in describing the Berry-Robnik formula  $P_{K=3}^{\text{BR}}(\rho_1, \rho_2, \rho_3)$  ( $\sum_{i=1}^3 \rho_i=1$ ). It is well known that the parameters  $\rho_i^q$  agree well with the classical ones  $\rho_i$  in the case of  $K=2$  [8–10,15,17]. However, relevant parameters in the case of  $K=3$  have not yet been checked numerically. We show that the quantum-mechanical information embedded in the energy level statistics enables us to determine the classical parameter  $\rho_i^*$  ( $i=1,2,3$ ). Here we derive the classical parameter  $\rho_i^*$  from the quantum-mechanical data of the level-spacing distribution  $P(S)$ .

We define the function  $I(y_1, y_2, y_3)$ ,

$$I(y_1, y_2, y_3) = \int_0^\infty |P(S) - P_{K=3}^{\text{BR}}(y_1, y_2, y_3; S)|^2 dS, \quad (3.6)$$

where  $\sum_{i=1}^3 y_i=1$ . The minimum of  $I(y_1, y_2, y_3)$  determines the best-fitting parameters  $\rho_i^*$  ( $i=1,2,3$ ) in the Berry-Robnik formula  $P_{K=3}^{\text{BR}}(y_1, y_2, y_3)$ , i.e.,

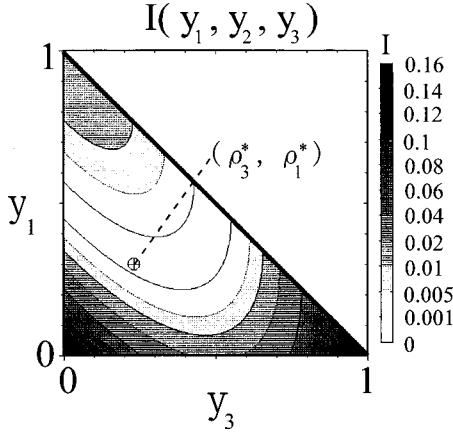


FIG. 14. Global aspect of the function  $I(y_1, y_2, y_3)$  at  $\delta = 0.445$ . The classical parameter ( $\rho_1^* = 0.30$ ,  $\rho_3^* = 0.232$ ) is observed in the narrow region minimizing the function  $I(y_1, y_2, y_3)$ .

$$I(\rho_1', \rho_2', \rho_3') = \min_{y_i} I(y_1, y_2, y_3). \quad (3.7)$$

Figure 14 reveals the global behaviors of  $I(y_1, y_2, y_3)$  on the two-dimensional plane  $(y_1, y_3)$ , where the value of  $I(y_1, y_2, y_3)$  is shown by contour lines with gray scales. Though those minimum points  $\rho_i'$  ( $i = 1, 2, 3$ ) which are defined by Eq. (3.7) and obtained numerically are fluctuating because of the finiteness in numerical data of  $P(S)$ , one can estimate the probable values of  $\rho_i'$ 's within the narrow band in two-dimensional space  $(y_1, y_3)$ . It is impossible to determine  $\rho_i'$  ( $i = 1, 2, 3$ ) without a large number of energy levels. The striking point is that the classical-mechanical quantity  $\rho_i^*$  is well approximated by the value of  $\rho_i'$ ,

$$\rho_i' \approx \rho_i^*. \quad (3.8)$$

The method based on Eqs. (3.6) and (3.7) enables us to obtain the classical parameters  $\rho_i^*$  in principle, since the formula  $P_{K=3}^{\text{BR}}(y_1, y_2, y_3)$  is unique at each point on the two-dimensional  $(y_1, y_3)$  plane. Figure 13(b) shows values of  $\rho_3'$  determined from the minimum point of  $I(\rho_1^*, y_2, y_3)$  on.

#### IV. SUMMARY AND DISCUSSIONS

In the present paper, by using oval billiards, we elucidated the effect of bifurcations in classical-mechanical systems on the statistics of the energy levels. We have shown that the Berry-Robnik distribution for one chaotic component approximates very well the nearest level-spacing distribution of a quantum oval billiards, and hence the two parameters are determined numerically. Thus we used the Berry-Robnik parameter as the measure of the effect of bifurcations on the nearest level-spacing distributions in oval billiards. The Berry-Robnik parameter suddenly decreased just at the point of bifurcation. We have also shown that the Berry-Robnik formula works very well when the number of chaotic components is taken precisely into consideration, and especially in the case of two chaotic components. Therefore, we checked, using numerical calculations, the conjectures proposed by Percival [27] and Berry and Robnik [7] in more than one chaotic component. It should be noted that one can detect the occurrence of bifurcation in the classical-

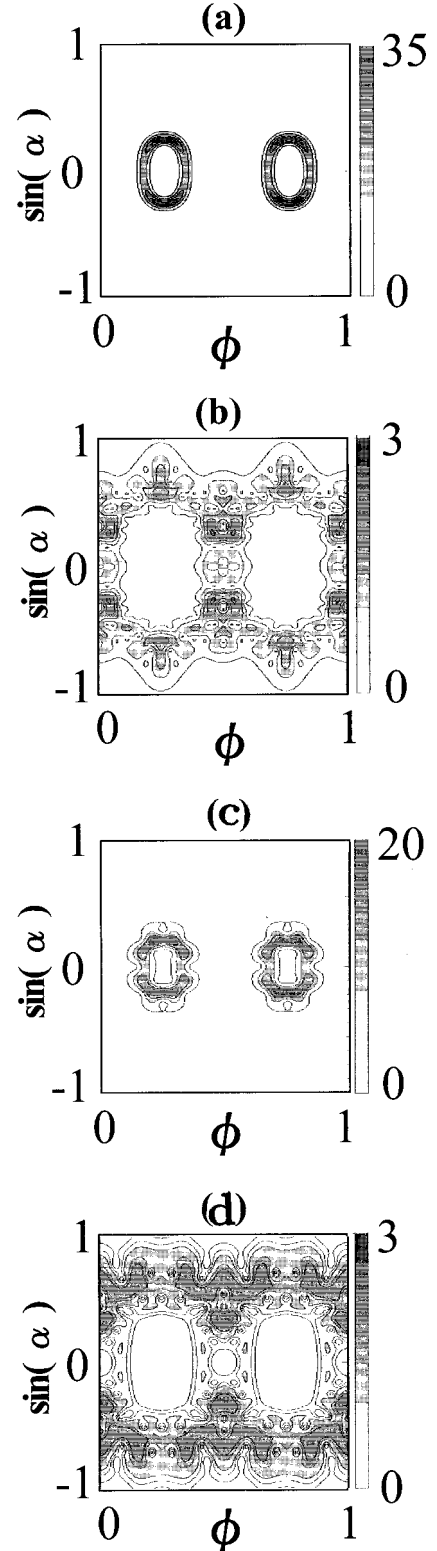


FIG. 15. (a) and (b) are the contour plots of the Husimi function  $\varrho_n(\phi, \sin \alpha)$  for typical eigenstates [(a)  $A^{1/2}k_n = 238.19$  and (b)  $A^{1/2}k_n = 238.24$ , where  $k_n = (2mE_n)^{1/2}/\hbar$  and  $A$  is area of the billiard] at  $\delta = 0.39$ . Each localizes in regular and irregular component, respectively. (c) and (d) are the contour plots of the Husimi function  $\varrho_n(\phi, \sin \alpha)$  for typical eigenstates [(c)  $A^{1/2}k_n = 132.51$  and (d)  $A^{1/2}k_n = 131.85$ ] at  $\delta = 0.44$ . Each localizes in the second or in the first irregular component, respectively. The Husimi function is scaled to satisfy the normalization condition  $\int_0^1 d\phi \int_{-1}^1 d\sin \alpha \varrho_n(\phi, \sin \alpha) = 1$ .

mechanical systems from the level-spacing distributions of the corresponding quantum systems. Our findings in this paper are all based on the numerical calculations, but the quantum-classical correspondence in the level-spacing distribution is completely satisfied in a wide parameter region with complex bifurcations.

In this paper, we dealt with the energy levels  $n = 400, \dots, 14\,400$  for calculation of the level-spacing distributions around the bifurcation point  $0.41 \leq \delta \leq 0.48$ , and hence the effective Planck constants are  $h_{\text{eff}} = 1/\sqrt{n} = 0.0083, \dots, 0.050$  [16], where  $A$  is area of the billiard and  $E_n$  is the  $n$ th eigenenergy. Quantum mechanics describes the structures beyond the scale  $h_{\text{eff}}$  of the classical phase space. In particular, the approximate size of the second chaotic component ( $\rho_3 \approx 0.25$  at the bifurcation point  $\delta = \delta_{c2}$ ) is larger than the effective Planck constant ( $\rho_3 > h_{\text{eff}}$ ), so that one can expect to observe the localization of wave functions in the second chaotic component over in the neighborhood of the bifurcation point, which will reflect to the third argument  $\rho_3^*$  in the Berry-Robnik formula. Here, let us introduce the phase-space representation of eigenstates by the Husimi function. We have employed the formalism of the Husimi function for the Birkhoff coordinates  $(\phi, \sin \alpha)$  defined in [29,30]. Figures 15(a) and 15(b) show contour plots of the Husimi functions  $\varrho_n(\phi, \sin \alpha)$  for two typical eigenstates in the case  $\delta = 0.39$ . One can see that each eigenstate clearly localizes either in a regular region or an irregular one before the second chaotic region appears ( $\delta < \delta_{c1}$ ). On the other hand, Figures 15(c) and 15(d) show the contour plots of the Husimi functions at  $\delta = 0.44$ , where the second chaotic region exists. Figure 15(c) reveals the eigenstate which localizes in the second chaotic component, and another localization in the first chaotic component is shown in Fig. 15(d). Two types of localization mentioned above are observed in the whole energy range which we studied, and the lack of mutual overlap between their eigenstates seems to guarantee the use of the Berry-Robnik formula for our system [14,18,19].

The assumptions used in the derivation of the Berry-Robnik formula have not yet been validated from theoretical viewpoints, although there is much numerical evidence for the case of one chaotic component; Bohigas, Tomsovic, and Ullmo analyzed a two-dimensional system of two coupled one-dimensional quartic oscillators [12], and numerically

verified the validity of the Percival conjecture [27]. Using the presence of the mechanical quasidegeneracy, they separated the energy levels into regular and irregular subclasses. Jacquod and Amiet [13], Li and Robnik [19], and Prosen [18] also separated the energy levels into regular and irregular subclasses, and analyzed substatistics for each class in order to check the Berry-Robnik conjecture [13]. Furthermore, Prosen and Robnik [10,14] and Carlo, Vergini, and Fendrik [17] estimated the semiclassical convergence of the level-spacing distributions to the Berry-Robnik formula by precisely using a large number of energy levels in an extremely deep semiclassical regime. In this paper, we have shown that the Berry-Robnik formula works very well, even in the case of two chaotic components, and follows the detailed structure of complex bifurcations in classical-mechanical systems.

The studies of the level statistics in nonlinear systems have been provided in another context in terms of the Brody distribution [6,30]. Terasaka and Matsushita studied the level statistics for one parameter family of coupled Morse-oscillator systems, and found that the Brody parameter reveals oscillatory changes in a wide parameter region. However, the oscillations were smooth, and hence no sudden change occurred in the Brody parameter. By using the Berry-Robnik formula for one chaotic component, we found the striking effect of bifurcations corresponded to the sudden change of the values of the Berry-Robnik parameter. In addition, Prosen has shown that the Berry-Robnik formula approximates numerical data in the far semiclassical regime better than the Brody distribution does [18]. Therefore, the Berry-Robnik formula is an adequate measure for the effect of the bifurcations in the semiclassical regime.

#### ACKNOWLEDGMENTS

The authors thank Professor T. Prosen and Dr. Y. Shimizu for fruitful discussions and valuable comments. T.H. is grateful to Dr. B. Komiyama and Dr. N. Egami for their continuous interest and encouragement. This research was supported by a Grant-in-Aid for Scientific Research (c) (09640472) from the Ministry of Education, Science and Culture of Japan. The computation in this work has been done using the facilities of the Supercomputer Center, Institute for Solid State Physics, University of Tokyo.

- 
- [1] M. V. Berry and M. Tabor, Proc. R. Soc. London, Ser. A **356**, 375 (1977).
  - [2] G. Casati, B. V. Chirikov, and I. Guarneri, Phys. Rev. Lett. **54**, 1350 (1985).
  - [3] O. Bohigas, M. J. Giannoni, and C. Schmidt, Phys. Rev. Lett. **52**, 1 (1984).
  - [4] M. Robnik, J. Phys. A **17**, 1049 (1984).
  - [5] T. H. Seligman, J. J. M. Verbaarschot, and M. R. Zirnbauer, Phys. Rev. Lett. **53**, 215 (1984).
  - [6] T. Terasaka and T. Matsushita, Phys. Rev. A **32**, 538 (1985).
  - [7] M. V. Berry and M. Robnik, J. Phys. A **17**, 2413 (1984).
  - [8] H. D. Meyer, E. Haller, H. Koppel, and L. S. Cederbaum, J. Phys. A **17**, L831 (1984).
  - [9] D. Wintgen and H. Friedrich, Phys. Rev. A **35**, 1464 (1987).
  - [10] T. Prosen and M. Robnik, J. Phys. A **27**, 8059 (1994).
  - [11] T. H. Seligman and J. J. M. Verbaarschot, J. Phys. A **18**, 2227 (1985).
  - [12] O. Bohigas, S. Tomsovic, and D. Ullmo, Phys. Rev. Lett. **64**, 1479 (1990).
  - [13] P. Jacquod and J. P. Amiet, J. Phys. A **28**, 4799 (1995).
  - [14] M. Robnik and T. Prosen, J. Phys. A **30**, 8787 (1997).
  - [15] T. Prosen and M. Robnik, J. Phys. A **26**, 2371 (1993).
  - [16] T. Prosen, J. Phys. A **31**, 7023 (1998).
  - [17] G. Carlo, E. Vergini, and A. J. Fendrik, Phys. Rev. E **57**, 5397 (1998).
  - [18] T. Prosen, Physica D **91**, 244 (1996).

- [19] B. Li and M. Robnik, *J. Phys. A* **28**, 4843 (1995).  
[20] G. Benettin and J. M. Strelcyn, *Phys. Rev. A* **17**, 773 (1978).  
[21] H. Henon and J. Wisdom, *Physica D* **8**, 157 (1983).  
[22] L. A. Bunimovich, *Funct. Anal. Appl.* **8**, 254 (1974).  
[23] G. D. Birkhoff, *Dynamical Systems* (American Mathematical Society, Providence, RI, 1927; reprinted 1996).  
[24] T. Harayama and Y. Aizawa, *Prog. Theor. Phys.* **84**, 23 (1990).  
[25] M. V. Berry and M. Wilkinson, *Proc. R. Soc. London, Ser. A* **392**, 15 (1984).  
[26] S. Tasaki, T. Harayama, and A. Shudo, *Phys. Rev. E* **56**, R13 (1998).  
[27] I. C. Percival, *J. Phys. B* **6**, L229 (1973).  
[28] M. V. Berry, *Philos. Trans. R. Soc. London, Ser. A* **287**, 237 (1977).  
[29] B. Crespi, G. Perez, and S-J. Chang, *Phys. Rev. Lett.* **47**, 986 (1993).  
[30] Y. Shimizu and A. Shudo, *Chaos Solitons Fractals* **5**, 1337 (1995).